



Short-term earthquake prediction in Kamchatka using low-frequency magnetic fields

A. Schekotov¹ · D. Chebrov² · M. Hayakawa^{3,4} · G. Belyaev⁵ · N. Berseneva⁶

Received: 14 March 2018 / Accepted: 17 December 2019 / Published online: 23 December 2019
© Springer Nature B.V. 2019

Abstract

This paper is devoted to a method of short-term earthquake (EQ) prediction in Kamchatka, Russia. Properties of low-frequency magnetic fields are the basics of the method, and we used two seismo-electromagnetic phenomena in the EQ prediction: 1. seismo-ionospheric depression in the frequency range of 0.01–0.1 Hz (ULF depression), 2. seismo-atmospheric radiation in the frequency range of 1–30 Hz (ULF/ELF radiation). It is now generally accepted that gas eruption before an EQ causes these ULF/ELF phenomena. We propose a hypothesis that gas emanates from the area in the bottom of Kuril–Kamchatka or Aleutian trenches closest to the epicenter of a forthcoming EQ. The three parameters of an EQ are (i) when (time), (ii) where (position) a next EQ is coming with (iii) how big (magnitude) in the short-term EQ prediction. Position of the source of atmospheric radiation gives an estimate of the epicenter location. Then, we estimate the local magnitude in consequence of its statistical dependence on ULF depression and epicenter distance. Date of a coming EQ is determined by the statistical dependence of delays of EQs relative to the dates of their precursors. The result of application of this method to real magnetic field data is illustrated by official prediction processes during a period of March–May 2016. Limits and possible errors of the method as well as methods to enhance the reliability of the prediction are discussed.

Keywords Earthquake (EQ) prediction · Seismo-electromagnetic phenomena · EQ preparation process · Lithosphere–atmosphere–ionosphere coupling · Subduction zone · Gas emanation

1 Introduction

The main purpose of this article is to show a possibility of estimating main parameters of a forthcoming earthquake (EQ) and try to answer the “eternal” question about the possibility of short-term prediction of EQs (Geller et al. 1997; Gufeld et al. 2011). This question was brought about many years ago after multiple abortive attempts to realize EQ prediction. During first years of investigations, these failures are caused by misconception that

✉ A. Schekotov
oldresident@yandex.ru

Extended author information available on the last page of the article

prediction is possible to provide only by means of seismic methods. However, during the course of time, a concept about seismic processes was changed and some doubts occurred concerning such a possibility. It became clearly necessary to use other phenomena: level of water table, temperature, gas consistency, animal behavior, moving of the Earth surface and different effects in electric and magnetic fields (Varotsos and Alexopoulos 1984; Varotsos et al. 1986; Molchanov and Hayakawa 2008; Hayakawa 2015). The last idea on electromagnetic phenomena gained recognition, especially because the possibility of using seismic electric signals (SES) for EQ prediction was shown (Varotsos and Lazaridou 1991; Varotsos et al. 1993, 2003), and ultra-low frequency (ULF) seismo-magnetic emissions were discovered for the Loma Prieta (Fraser-Smith et al. 1990), Spitak (Kopytenko et al. 1990; Molchanov et al. 1992), Guam (Hayakawa et al. 1996) EQs. However, most efforts on ULF radiation to replicate these results were not so successful in spite of further works (e.g., Hattori 2013). This is the reason why Japanese and Russian specialists founded in 1999 a complex geophysical observatory Karymshina in the Kamchatka peninsula (Uyeda et al. 2002). Because we observe low industrial interferences and a rather high level of seismic activity there, this observatory creates good conditions for the observation of different seismo-electromagnetic phenomena. For this aim, as one of many devices, we have installed a three-component induction magnetometer in the frequency band of 0.003–30 Hz.

After 5 years of investigations, we have found two important and interesting phenomena, which could be applied for short-term EQ prediction. The first of them is a phenomenon of seismo-ionospheric depression (decreasing) of ULF magnetic field at the frequency 0.01–0.1 Hz (Schekotov et al. 2006). The second is ULF/ELF radiation at the frequency of 1–30 Hz (Schekotov et al. 2007). We have then assumed that the cause of ULF depression is ionospheric inhomogeneity (perturbation) (as is conventionally observed by sub-ionospheric VLF propagation Hayakawa et al. 2010) and the origin of ULF/ELF radiation is electric discharges in the atmosphere (Schekotov et al. 2013) and both phenomena are caused by acoustic gravity waves excited by gas eruption. We also used here an index of local seismicity, which depends both on the magnitude of EQ and on its epicenter distance. Based on four-year statistics, we have shown the proportionality of this index to the maximal preceding EQ depression. We have shown the locality and stationarity of both phenomena and their reliability for decisive EQ prediction problem.

Here, we describe our method of predicting main parameters of EQs in Kamchatka based on those phenomena and data obtained in the last experiment covering an interval from December 2014 to September 2017. We should note that our data acquisition system did not work every year approximately from the beginning of May till November when night temperature was positive, probably because it may be caused by galvanic processes in some connector(s) (sensors and cables lying underground from June 1999). Based on the data during the first period until March 2016, we were accumulating the statistics of dependence of local seismicity index on maximum value of preceding ULF depression.

We should make some assumptions to determine the epicenter position of a forthcoming EQ and its magnitude. For this purpose, it has been hypothesized that gases are lifting from the area in the bottom of Kuril–Kamchatka or Aleutian trench closest to the epicenter of a forthcoming EQ and then they are coming out onto the ocean surface. The forthcoming EQ should occur somewhere in this area opposite to the direction of peninsula or Commander Islands. We also assumed that the source of atmospheric ULF/ELF radiation and the position of ionospheric inhomogeneity, which cause ULF depression, are located above this same region. Then, we have considered all EQs occurred, which had reliable well-separated precursors. Thereafter we computed distributions of delays of dates of main shocks

behind dates of maximum of observed precursors depending on local magnitude. They give us information on a probable time interval of a forthcoming EQ.

Design of the experiment, procedures of data processing and procedure of EQ prediction will be presented in the second section. Then, in the third section, we will exhibit examples of the EQ prediction based on a few events, which occurred from March to May 2016. The fourth section is devoted to the discussion of this method and considerations concerning a possibility to enhance the prediction accuracy.

2 Data collection and processing

2.1 Design of the experiment

We study a possibility of EQ prediction in the observatory Karimshina (Kamchatka, Russia, geographic latitude 52.83° N, longitude 158.13° E) from the year of 2000 until present. There are two stages of investigations. First one till about the year of 2005 was devoted to looking for different types of electromagnetic precursors. As a result, we have found two most reliable ones and studied their properties. During the last stage from December 2013 until present, we focus on the investigation of prediction methods utilizing those phenomena we found. We began an official prediction of Kamchatka EQs from March 2016.

This Kamchatka region has two advantages—high seismic activity and low level of industrial interferences. Figure 1 displays a map of this region with EQs occurred from December 2014 to September 2017 and whose local magnitude exceeded 5.0. A black rectangular and a rhomb depict Petropavlovsk-Kamchatsky and the observatory Karimshina here accordingly. Kuril–Kamchatka and Aleutian trenches are the boundaries

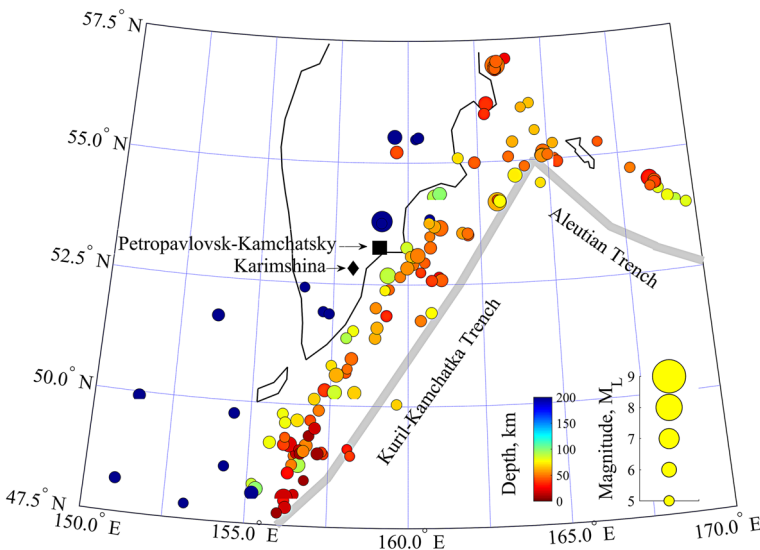


Fig. 1 Map of Kamchatka region with EQs with $M_L > 5$ occurred during 12/01/2014–09/30/2017. They are marked by color circles, and their color depends on the focus depth and the diameter depends on the magnitude. Thick gray lines show the axes of Kuril–Kamchatka and Aleutian trenches

of two zones of subduction, and the gray thick lines show their axes. The color bar in the right bottom of the map shows the correspondence of the EQ depth. Panel on the right with yellow circles reflects the correspondence between the diameter of circles and EQ local magnitudes. As is seen in Fig. 1, most of EQ epicenters lie between the Kuril–Kamchatka trench and coast of peninsula and Kuril Islands and along Commander Islands in the Northeast. Deepest EQs occur under the surface peninsula and in the Sea of Okhotsk.

Magnetic field variations are measured by means of the three-component induction magnetometer at frequencies of 0.003–40 Hz, with noise level $0.16F^{-1}$ pT/Hz $^{-1/2}$ and conversion function $0.4 F \text{ Hz} \cdot \text{V/nT}$ in the frequency band $F=0.003\text{--}4$ Hz and 1.6 V/nT in the band $F=4\text{--}40$ Hz. The sensors H and D for horizontal field components are oriented along the magnetic meridian and transversally to it, and the Z sensor is vertical. They are enclosed in a concrete box with dry sand to suppress seismic, wind, acoustic interferences and to decrease weather influence. The parameters of all sensors are identical with deviations less than 3% in absolute values of the conversion function and 2° in phase. These discrepancies can be corrected with the help of calibration circuits. Figure 2 illustrates the block diagram of data collection and processing procedure. The signal is fed to the data acquisition system (DAS) GSR-24 with the sampling rate of 100 Hz (in 24 bits) (<http://www.seismicsystems.net/products/digitizers.html>).

Then, data are transmitted through Wi-Fi channel to a computer at the observatory, which realizes their temporary storage. Then, once a day they are fed through Internet to the computer of Kamchatka Branch of Geophysical Survey, RAS located in Petropavlovsk-Kamchatsky. This applied equipment provides us with a possibility to collect and store a large volume of data, to realize their preliminary analysis and to provide daily access to them through FTP server. Final processing of these data is carried out in Institute of Physics of the Earth, RAS in Moscow. Copies of results of processing are sent back to an FTP server at Kamchatka. The conclusion about a seismic danger for Kamchatka region is sent to the commission on EQ prediction in Kamchatka Branch of Geophysical Survey RAS. This procedure is taken every week or more often, depending on the local seismic activity. This conclusion consists of the description of temporal evolution of magnetic field variations with graphical illustrations and estimation of the magnitude, location and time of a forthcoming EQ.

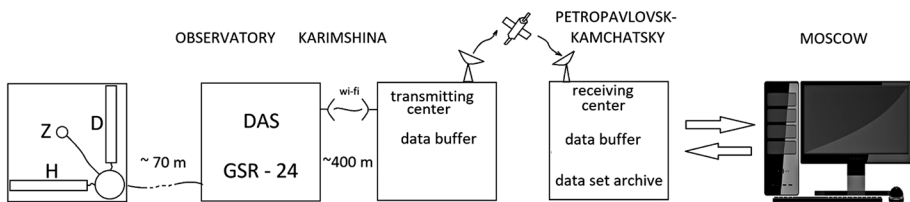


Fig. 2 Block diagram of data collection and processing procedure. Left rectangular is a box with sensors, next one—data acquisition system housing in a small shelter. Then, the signal through Wi-Fi transmitting in the computer which is located in the building of the observatory and then transmitting in Petropavlovsk-Kamchatsky where obtained data are stored, preliminarily processed and put on an ftp server which provide 2-directional real-time access. Then, they are transmitted to Moscow for providing their processing and analysis result

2.2 Estimation of local seismicity

We estimate the local seismicity by an index K_{LS} ,

$$K_{LS} = \frac{10^{0.75M_L}}{10(R + 100)} \tag{1}$$

where R is the distance from the observational point to epicenter (in km) and M_L is local EQ magnitude. Molchanov and Hayakawa (2008) introduced the similar index to study seism-acoustic emissions. In this index, they take into account the attenuation of seismic waves in Earth’s crust, even though it is not needed in our case because low-frequency waves propagate in the Earth–ionosphere waveguide with very small damping.

Figure 3 illustrates the evolution of local seismicity during the same period as shown in Fig. 1. This representation gives a possibility to compare EQs in time domain, which shows intervals with different degrees of seismic activity.

The most important property of K_{LS} consists in its relation with characteristics of magnetic field before an EQ, which leads to a possibility to predict the magnitude of a forthcoming EQ. We will consider it in details in Sect. 2.4

Hereinafter, we will use the notations R_{min}^r , R_{mean}^r and R_{max}^r for minimum, mean and maximum distances of the radiation source, K_{LS}^r for estimation of the local seismicity index through radiation characteristics and M_L^{pr} for the notation of predicted local EQ magnitude.

2.3 Estimation the position of epicenters

Earlier, we established that the azimuth of source of ELF radiation rarely coincides with that of the epicenter of a forthcoming EQ and does not give any information concerning the position of epicenters (Schekotov et al. 2008). So here, we utilize a new approach to estimate the position of EQ epicenters. The main assumption of this method is concerned with the position of the source of radiation. We have hypothesized that the cause of radiation is acoustic gravity waves, which are generated by eruption of gases from an EQ source. That is, they come out in the ocean along the boundaries of tectonic plates in Kuril–Kamchatka and Aleutian trenches, and then they reach the surface of ocean and lead to the generation of acoustic and gravity waves, which cause the charge separation in the atmosphere, resulting in intra- and inter-cloud electric discharges and observed radiation. Position of its source can be determined as an intersection of main lobes of azimuthal distribution of radiation and axes of trenches.

The azimuth α of the radiation source is determined as the angle between the north direction and perpendicular to the main axis of the ellipse of polarization.

$$\alpha = 180 - \theta \tag{2}$$

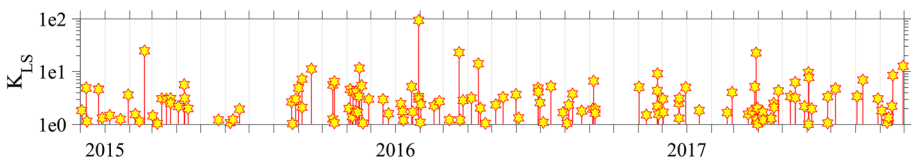


Fig. 3 Evolution of seismic activity for the interval of 12/01/2014–09/30/2017 represented by the index of local seismic activity K_{LS}

Here θ is the angle, which the major axis of the ellipse makes with the direction of the D field component. It is calculated through the instantaneous amplitudes A_h , A_d and phases φ_h , φ_d (Fowler, et al. 1967) of the complex signal, which are obtained from the original signals by means of Hilbert transform. Previously original signals of the field components are filtered in the frequency range of 2–5 Hertz.

$$\tan(2\theta) = \frac{2A_d A_h}{A_d^2 - A_h^2} \cos(\phi_h - \phi_d) \quad (3)$$

Figure 4 illustrates the procedure of estimation of EQ epicenter position. The azimuthal distribution is represented in the form of circular histogram with 5° resolution, which is placed on the map in azimuthal equidistant projection. Center of the map coincides with the location of observatory Karimshina (KRM). Concentric circles display the distance from the observatory with a step of 100 km. A ring located at the edge of the panel reflects the cumulative azimuthal distribution observed during the previous week. Degree of blackness of its parts is proportional to the flux of pulses from this direction.

Black dashed lines show the boundaries of maximum flux of radiation, which is determined by azimuths of impulse fluxes exceeding a half of cumulative maximum value. We think that regions of radiation sources are located in intersections of largest radiation and axes of trenches. Thick green lines mark locations of these regions. The blue arrow displays the distance R_{mean}^r between the observatory KRM and middle point of the nearest zone

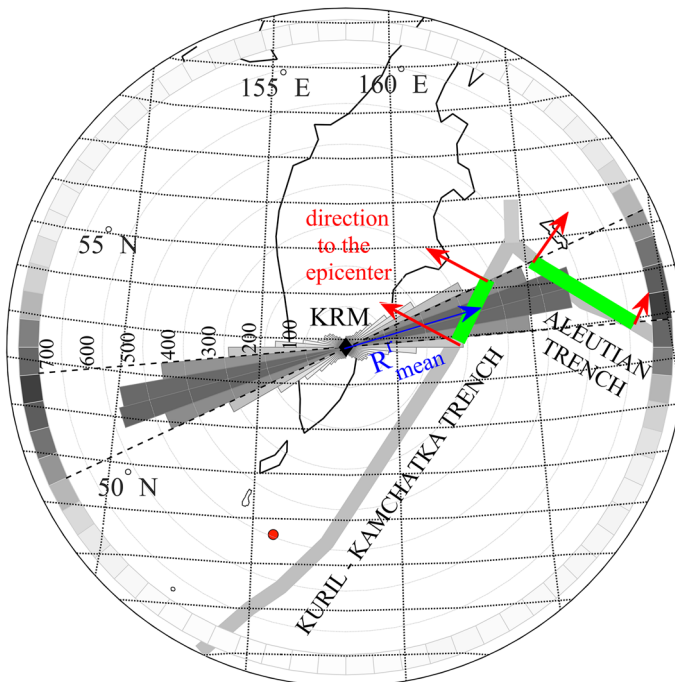


Fig. 4 Map of region with azimuthal distributions of radiation observed on a particular day of April 11, 2016. Thick green lines display probable sources of radiation. A blue arrow depicts the mean distance to the nearest one. Red arrows illustrate the direction to a possible position of epicenters. R_{mean}^r —mean distance to the source of radiation

of radiation. Just the same, we determine R_{max}^r and R_{min}^r as distances until the distant and nearby boundaries. They are equal to, $R_{min}^r \simeq 280$ km, $R_{mean}^r \simeq 330$ km and $R_{max}^r \simeq 380$ km. The equidistant circles were used for estimating these values. Just the same, we can estimate distances for the second green line on the Aleutian trench.

Red arrows show probable directions to the epicenters of a forthcoming EQ. A single site of observation is not able to provide always a well-defined answer concerning the direction to the epicenter. In the presented case, it may be the region of peninsula Kamchatka or Aleutian’s islands. Moreover, this method cannot determine an exact position of a forthcoming EQ. It can define only latitudes where it can occur. Inasmuch as most of EQs occur in ~200 km zone between the coast and axis of trench (e.g., see Fig. 1), we can estimate probable epicenter locations of future events. The nearest boundary of green line determines one of latitude boundaries. In this case, it is equal to ~53° N. Another boundary is the latitude of the point located at distance ~200 km perpendicular to the farther boundary in green line. It is equal to ~54.5° N. Mean latitude $\simeq 53.75^\circ$ N and as a result, predicted latitudes: $Lat^{Pf} = 53.75 \pm 0.75^\circ$ N. Just the same, we could estimate latitudes for probable Aleutian EQs and their probable minimum, mean and maximum distances until the epicenter of a coming EQ. They are approximately equal to appropriate distances to the region of radiation source. It is right for nearest events but may lead to noticeable errors for large distances from trenches.

2.4 Prediction of local magnitude

The main purpose of this section is to show how to predict value of the local magnitude M_L using characteristics of low-frequency magnetic field. A relatively new phenomenon of seismo-ionospheric ULF depression provides us with a possibility to predict M_L on the basis of statistical dependence of ULF depression on local seismicity K_{LS} (Schekotov et al. 2006). This phenomenon consists in reduction in magnetic field variations at frequencies < 1 Hz during a few days–weeks before an EQ.

Here, we consider daily and hourly ULF depressions. Daily ULF depression is determined as a maximum of all hourly depressions. Hourly depression is equal to the maximum of inverse value of element-wise multiplication of the frequency vector and one-hour averaged spectral density. They are calculated for both components as follows:

$$Dep_H = \max \left(\frac{1}{f \langle P_{hh} \rangle_t} \right)_f \tag{4}$$

$$Dep_D = \max \left(\frac{1}{f \langle P_{dd} \rangle_t} \right)_f \tag{5}$$

where P_{hh} and P_{dd} are power spectral densities of H and D components, and f —vector of central frequencies of spectral components.

The procedure of calculation of ULF depressions is as follows:

1. Decreasing the sampling frequency of initial signal from 100 to 1 Hz
2. Division of daily files on 47 hourly samples with overlapping of 30 min
3. Calculation of power spectral densities for these samples with resolution ~0.002 Hz using Welch method

4. Flattening (decreasing of slope) spectra by multiplying spectral components into their middle frequencies
5. Calculation of the hourly maximum depression by determining its maximum frequency component [Eqs. (4) and (5)]
6. Determining maximum daily depression as a maximum of 47 hourly maximum values.

Figure 5 illustrates the signal evolution (middle panel), hourly and daily maximum depressions (bottom panel) in conjunction with the evolution of local seismicity (top panel). Minimum field variations (2nd panel) and therefore maximum values of depression (gray bars on the bottom panel) are observed usually around local midnight (~ 13.5 h UT). The value of maximum daily ULF depression and its date are shown as well, because we will use them to estimate the magnitude and time of the coming EQ. We declare an alarm and begin waiting for a new EQ after the date with maximum daily depression.

Figure 6 displays the statistical relation between maximum of ULF depression and local seismicity for 26 events. We use a linear interpolation for the approximation of this dependence. The red line shows the mean value of this relationship. Three pairs of dashed lines show boundaries of 70%, 80% and 90% confidence intervals. The ordinates of color circles in the

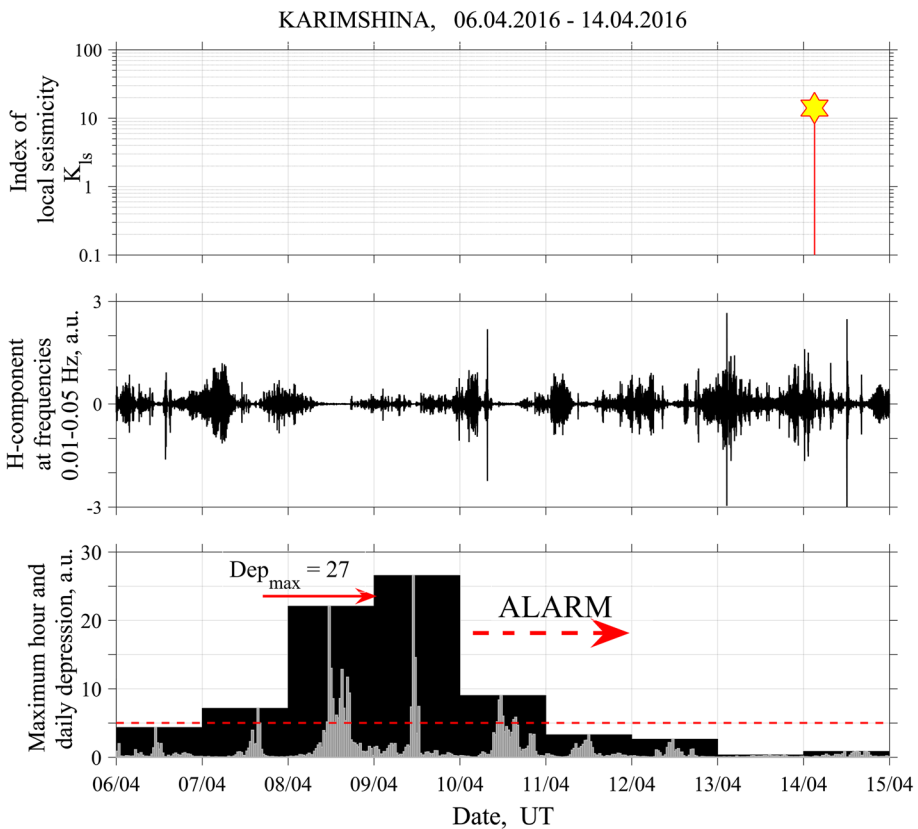


Fig. 5 Top panel exhibits the evolution of local seismicity, next panel shows magnetic field variations and bottom panel illustrates the evolution of maximum hourly values of ULF depression depicted by gray bars and maximum daily values displayed by black bars

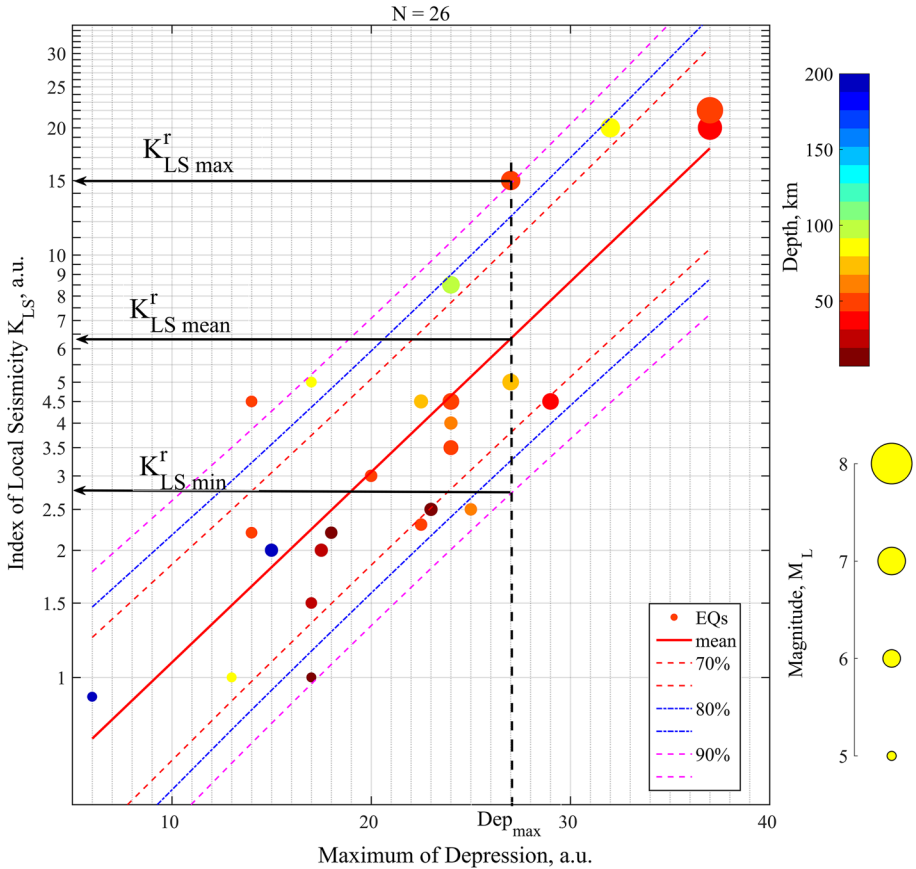


Fig. 6 Statistical dependence of local seismicity index on maximum ULF depression. A red line refers to the mean value, and three pairs of dashed lines show boundaries of 70%, 80% and 90% confidence intervals. Their intersections with a vertical dashed line are equal to minimum K_{LS}^r min, mean K_{LS}^r mean and maximum K_{LS}^r max values of local seismicity index calculated through parameters of radiation. This line begins from the value equal to Dep_{max} on the horizontal axis

top panel exhibit values of index of local seismicity K_{LS} of observed EQs with respect to the max value of preceding daily ULF depression Dep_{max} (e.g., see Fig. 5). Their dimension and color depend on the magnitude and depth of hypocenter, respectively, and two plots on the right illustrate these relations. Possible minimum, mean and maximum values of K_{LS}^r are shown for considered EQs with $M_L = 6.2$ occurred on 14 April 2016.

An expression for estimation of predicted local magnitude M_L^{pr} obtained through the low-frequency radiation is derived from Eq. (1) using K_{LS}^r and R^r :

$$M_L^{pr} = (\log 10(K_{LS}^r)) + 1 + \log 10(100 + R^r)/0.75 \tag{6}$$

where K_{LS}^r and R^r are the following vectors (see Figs. 4 and 6):

$$K_{LS}^r = [K_{LS}^r \text{ min } K_{LS}^r \text{ mean } K_{LS}^r \text{ max}] \tag{7}$$

$$R^r = [R_{\max}^r \ R_{\text{mean}}^r \ R_{\min}^r] \quad (8)$$

We use the inverse order of distances in the vector R^r on the assumption that minimum and maximum values of K_{LS}^r correspond vice versa with maximum and minimum distances from the observatory to the region of radiation source. As for the considered EQ, after substitution of these values in Eq. (6) and after rounding the result down to one decimal place, we obtain the estimation of $M_{\text{L}}^{\text{pr}} = [5.6 \ 5.9 \ 6.2]$ or $M_{\text{L}}^{\text{pr}} = 5.9 \pm 0.3$ with probability 80% and $M_{\text{L}}^{\text{pr}} = 5.9 \pm 0.4$ with probability 90%.

2.5 Detection of the radiation

After having examined different characteristics devoted to the detection of ULF/ELF radiation, we have proposed a new combined characteristic parameter ΔS in order to detect seismo-atmospheric ULF/ELF radiation (Schekotov et al. 2007; Schekotov and Hayakawa 2017), which is given by Eq. (9):

$$\Delta S_{\text{EW}} = \frac{\frac{P_{hh}}{P_{dd}} - 1}{\text{rms}(\tan \beta)} \quad (9)$$

A success in the application of this parameter ΔS_{EW} is partly because a majority of nearby EQs take place east of our station. In order to detect radiation from all directions, we added a similar characteristic ΔS_{NS} for the orthogonal direction:

$$\Delta S_{\text{NS}} = \frac{\frac{P_{dd}}{P_{hh}}}{\text{rms}(\tan \beta)} \quad (10)$$

The numerator contains the ratio of two horizontal spectral components P_{hh} (NS component of magnetic field) and P_{dd} (EW component). The denominator is the root-mean-square (rms) of the deviation of signal ellipticity. Equation 11 gives the expression of β :

$$\beta = \frac{1}{2} \arcsin \left\{ \frac{\text{Im}(P_{dh} - P_{hd})}{[(P_{hh} - P_{dd})^2 + 4P_{hh}P_{dd}]^{1/2}} \right\} \quad (11)$$

Here P_{dh} and P_{hd} are cross-power spectral densities, and Im means imaginary part. Schekotov et al. (2007) have found an enhancement in the spectral ratio of P_{hh}/P_{dd} and a reduction in the standard deviation of ellipticity before an EQ, and the parameter introduced by Eq. (9) is proved to be most sensitive and reproducible to seismic shock. The ellipticity or the ratio of minor axis to major axis is defined by $\tan \beta$. The sense of polarization is characterized by the sign of β ; when $\beta > 0$, the polarization is right hand (RH), and $\beta < 0$ means the left-hand (LH) polarization. The linear polarization is expressed by $\beta = 0$ (Fowler et al. 1967).

The field power spectral densities P_{hh} , P_{dd} and their cross-power spectral densities P_{hd} , P_{dh} are calculated by using Fourier transform with frequency resolution of about 0.1 Hz. Spectral components in a frequency range from 0.1 to 30 Hz are taken into account. They are averaged over one-Hz intervals, so that we have 30 spectral components in the present analysis.

Thus, the sequence of processing for both components is as follows:

1. We divide the daily file into 3-hour intervals.
2. For every interval, we calculate spectral densities and find a maximal spectral component of $\Delta S(f)$. Gray bars reflect 3-hour maxima in Fig. 7
3. We find daily the maximum value of ΔS among all 3-hour values. Black bars depict daily maxima (see Fig. 7)

We also observe the pulse flux density in the bandpass of 3–5 Hz. It is calculated as a number of pulses per hour with peak power exceeding about 3–5 times the mean power of total signal. We consider only separated pulses with interval > 1 s. Figure 7 exhibits the evolution of both components of ΔS and pulse flux density in conjunction with local seismicity. We declare an alarm and begin waiting for a new EQ after the date with maximum daily ΔS .

2.6 Estimation of the occurrence time

The estimation of time of a forthcoming EQ is determined by statistical dependencies of their delays relative to the dates of maximum values of precursors—depression and ΔS . Top panels of Fig. 8 exhibit such dependence of probability (frequency of occurrence) of EQs depending on the delay time of EQ relative to the maximum of ULF depression (left) and maximum of ΔS (right). It is visible that most of events occur during 2–10 days after the maximum of precursors. However, we do not take into account the dependence delay on expected magnitude. This is considered on bottom panels. Left panel illustrates the

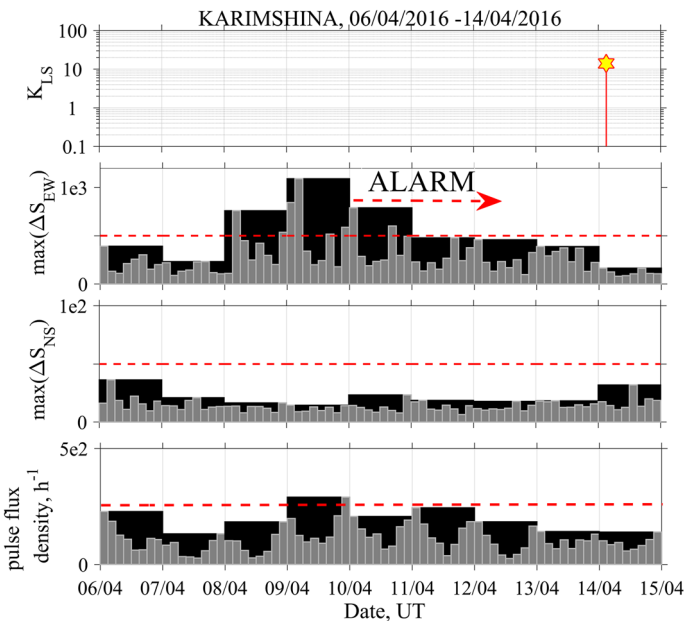


Fig. 7 Top panel illustrates the evolution of local seismicity represented by K_{LS} -index. Next two panels show the evolutions of maximum 3 hours and daily ΔS for both components of magnetic field. Bottom panel exhibits 3 hours and daily evolution of pulse flux density. For last three panels, gray bars refer to 3-hour values and black ones, daily values

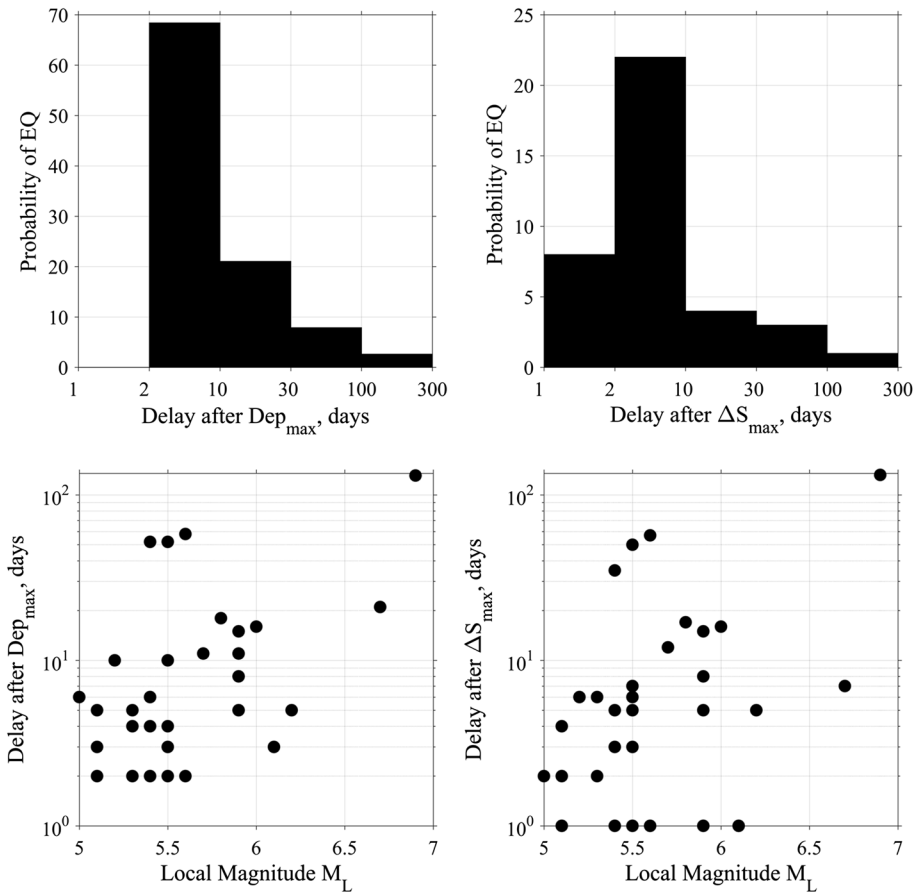


Fig. 8 Top panels exhibit the probability of EQ occurrence depending on the time after the date of Dep_{max} (left) and ΔS_{max} (right). Bottom panels display dependences of these delays on local magnitudes M_L

dependence on magnitude of lead time, the delay of an EQ behind the date of maximum depression. Right panels refer to the maximum ΔS . We do not observe here a very clear tendency of growth of delay with a growth in EQ magnitude. Rather weak statistics in most degree is explained by impossibility to reliably separate some precursors of different events using one point of observation.

2.7 Procedure of the prediction

The procedure of the prediction should provide the following information:

1. Warning about a forthcoming EQ,
2. Estimation of the epicenter position,
3. Estimation of the EQ magnitude,
4. Information about the EQ date,
5. Documentary notification of the special commission about a seismic danger,

6. Identification of a coming EQ with predicted parameters.

Procedure of the EQ prediction is based on the data represented in three main figures. One of them is daily updated figure like Fig. 9, which reflects the evolution of magnetic field characteristics and seismicity during the last 2 weeks. Another figure (Fig. 6) illustrates the statistical dependence of K_{LS} on maximum ULF depression. New events continually replenish its information. Third figure (Fig. 8) shows statistical dependencies of EQ dates behind dates of precursors. Let us illustrate this algorithm of the prediction by an example of EQ occurred on 14 April 2016 with local magnitude $M_L = 6.2$. Four steps of the prediction for this EQ are considered in previous sections. All these data and their representation on panels are described in previous sections.

Warning about a forthcoming EQ will be issued after passing the maximum of ULF depression (see Fig. 4 in Sect. 2.4) or ΔS (see Fig. 7 in Sect. 2.6) exceeding some threshold level (depicted by red dashed lines). This is the condition to declare an alarm, so that we should watch closely changes of magnetic field characteristics. We pay more attention to both components of ULF depression than ΔS because the latter is found to be a less sensitive detector of seismic events.

During the few nearest days, we should determine the position of the source of ULF/ELF radiation and its distance from the point of observation as described in Sect. 2.3. In our case, we obtained distance $R^r = 280 \pm 50$ km and predicted an interval of possible latitudes of the epicenter: $Lat^{Pr} = 53.75 \pm 0.75^\circ$ N.

The next step consists in the estimation of expected magnitude. Firstly, we determine values of indices of local seismicity $K_{LS \min}^r$, $K_{LS \text{ mean}}^r$ and $K_{LS \text{ max}}^r$ for maximum value

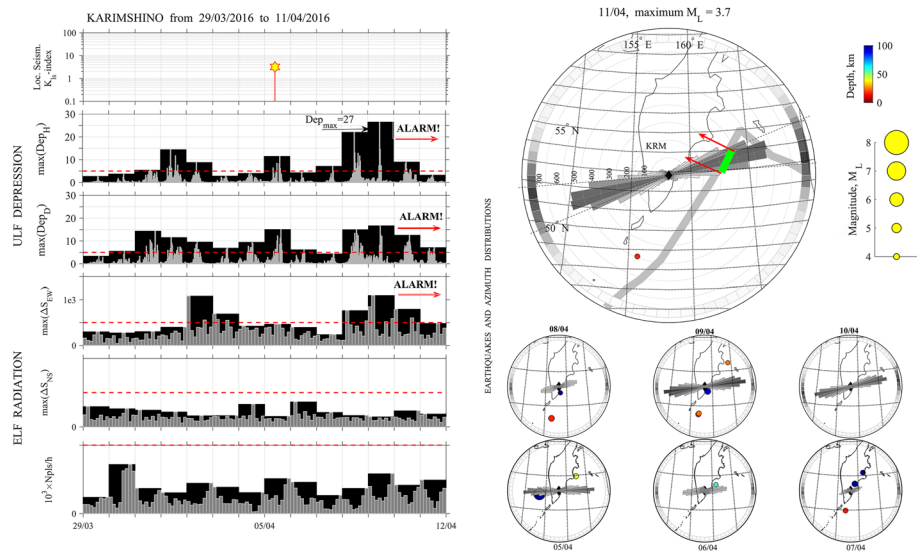


Fig. 9 Evolutions of characteristics of magnetic field and seismicity during 2 weeks. Top rectangular panel displays the evolution of local seismicity; next two rectangular panels show the evolution of ULF depression for both field components. Then, fourth and fifth panels illustrate the evolution of ΔS for both components, and bottom panel shows the evolution of pulse flux density. Right round panels show the evolutions of azimuthal distribution and seismicity placed on the map of region. Each round panel is based on the data during the last 7 days of observation

of depression and chosen confidence interval. Then, we can calculate the probable value of local magnitude as described in Sect. 2.4. We obtained the predicted local magnitude $M_L^{pr} = 5.9 \pm 0.3$ with probability 80%.

Lastly, we finish the forecast by estimating a *waiting interval*. It is determined from Fig. 8 in Sect. 2.6, which lies from 2 days to 2 months for an EQ with $M_L \sim 6$.

On the next stage, we should give the *official information* about a seismic danger in the special commission. It sums up predictions obtained from different sources and gives the conclusion.

The necessity of *identification* of the predicted EQ needs to exclude possible mistakes caused by overlapping of precursors of other events. An observing index of local seismicity K_{LS} lying in the predicted interval is one of evidences to expect an EQ. It should satisfy the condition: $K_{LS \min}^r < K_{LS} < K_{LS \max}^r$. Other sign of reliability is the position of epicenter of the observed event. It should be located in the prediction limits. Figure 10 illustrates such coincidence for an EQ which occurred on April 14 with $K_{LS} \sim 12$ and latitude of the epicenter $Lat = 53.66^\circ N$. Moreover, its magnitude $M_L = 6.2$ was also found to lie in the predicted limits.

An EQ occurred four days after the maximum ULF depression, on April 14, 2016, with local magnitude $M_L = 6.2$ at the latitude $Lat = 53.66^\circ N$. It is coincident with our prediction quite well. Figure 10 shows the temporal evolution of the same characteristics as in the previous figure, but during 2 weeks before the date of predicted EQ. Position of its epicenter is depicted by the largest circle placed in E-N direction from the point of observation KRM.

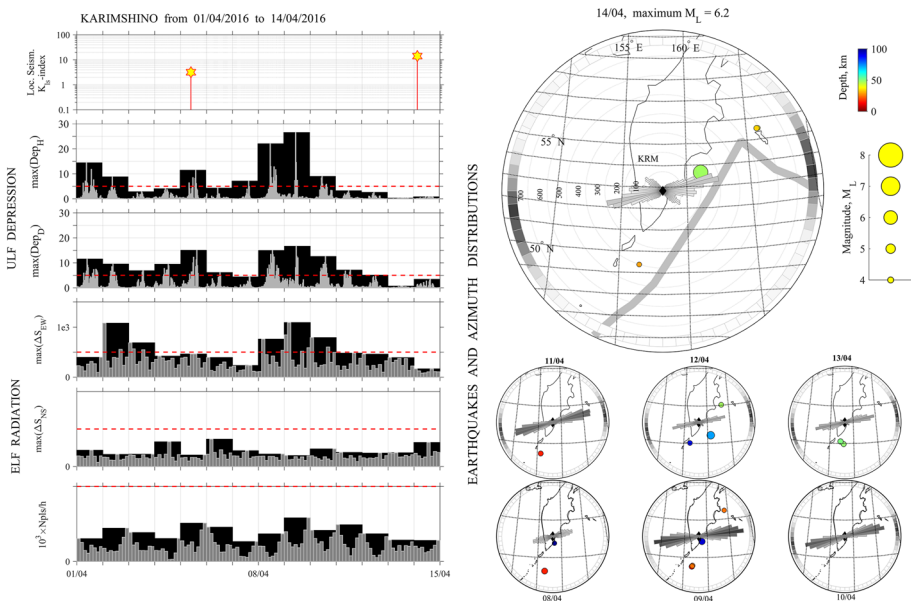


Fig. 10 Same as in the previous figure, but shifted up to the date of predicted EQ (14 Apr 2016)

3 Results

Here, we show results of the prediction for an interval from March 1 to May 10, 2016, and this was our first attempt in this experiment. It became possible when we understood that cumulated statistics (similar to Fig. 6) gives a possibility to estimate the magnitude of a forthcoming EQ with satisfactory accuracy. Last date of this interval was conditioned by a growth in inner interferences. This seasonal effect happens every year with growth of air temperature and probable increasing galvanic processes in connectors.

Figure 11 displays the evolution of seismicity. Top panel illustrates its evolution by the index of local seismicity K_{LS} . We marked magnitudes of sufficiently successful predicted EQs by red color, while other ones by blue color. Bottom panel illustrates the same, but in a spatial domain. EQs and their magnitudes and dates are shown on the map of region. Size of circles is proportional to the local magnitude, and their color depends on the depth of hypocenter. These relationships are depicted in the right of bottom panel.

Table 1 illustrates a comparison of characteristics of occurred EQs and predicted values of local magnitudes and latitudes. The first column refers to the sequence number of EQs, second column—their dates, third and fourth columns display real latitudes “Lat” and predicted latitudes “Lat^{pr}.” Next two columns refer to longitudes “Lon” and depths of hypocenters. Then, two columns display real magnitudes “ M_L ” and predicted local magnitudes

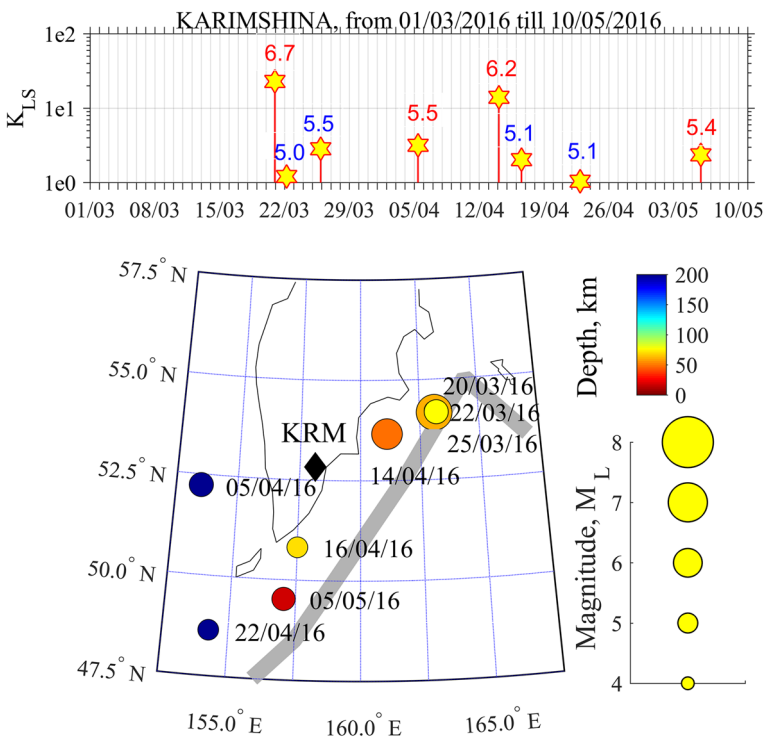


Fig. 11 Top panel shows the evolution of seismicity in time domain. Map on the bottom panel illustrates EQ epicenter positions by circles and their dates. It also shows EQ magnitudes by dimension of circles and their depth by color

Table 1 Results of the experiment on EQ prediction during March–May 2016

No.	Date	Lat	Lat ^{pr}	Lon	Depth	M _L	M ^{pr} _L	Distst.	Result	Comment
1	2016-03-20	54.14	53±1°	163.14	43	6.7	6.4±0.4	362	Predicted	
2	2016-03-22	54.21	n/d	163.13	44	5.0	n/d	364	Not predicted	Aftershock
3	2016-03-25	54.19	n/d	163.18	63	5.5	n/d	366	Not predicted	Aftershock
4	2016-04-05	52.23	53.5±1°	153.51	501	5.5	5.3±0.3	320	Predicted	Deep
5	2016-04-14	53.66	53.75±.75°	161.11	48	6.2	6.1±0.3	219	Predicted	
6	2016-04-16	50.82	n/d	157.50	69	5.1	n/d	468	Not predicted	Small, dist.
7	2016-04-22	48.64	n/d	154.26	197	5.1	n/d	539	Not predicted	Small, dist.
8	2016-05-05	49.53	49±1°	157.04	16	5.4	5.6±0.4	375	Predicted	

“ M_L^{PF} .” Next column “Dist” shows the distance from the observatory and next column is “Result,” which displays success in prediction. The last column “Comment” explains causes of not prediction—foreshocks, small events. We see that local magnitudes of four strongest main shocks have been well predicted. Predicted latitudes in a pair of cases (they are underlined) have unimportant errors for the first and the fourth events.

4 Discussion and conclusion

We have demonstrated a method of the short-term EQ prediction, or predicting three parameters of Kamchatka EQs. It provides us with the estimation of latitude and local magnitude of a forthcoming event. Moreover, it has an additional indicator ΔS of a coming EQ. Statistical dependence of delay of the forthcoming EQ behind the maxima of ULF depression and ΔS gives a possibility to determine the rough date of the forthcoming event. Consider all these properties separately.

Procedure of the prediction of EQ epicenter latitude was described in Sect. 2.3. It is based on the hypothesis that gases emanate from the preparation zone of EQ implicitly cause atmospheric radiation, which move along the boundary of continental and oceanic plates, reach the bottom of trench and lift in the surface of ocean. Here, they excite acoustic gravity waves. Last ones in the process of propagation modify the characteristics of atmosphere and lower ionosphere. Radon can also be another candidate of the atmospheric radiation (Pulinets et al. 2015). The most important consequence of that hypothesis is that the source of radiation is located in the atmosphere above axes of trenches, and this length can be determined by an intersection of main lobe of radiation with the axis of trench. Earlier we, without considerable success, tried to determine the EQ epicenter by assuming that the source of radiation is located in the region too (Schekotov et al. 2008). Figure 12 illustrates the correctness of our assumptions concerning the relative position of the sources of radiation and epicenter. It displays eight maps with color circles, which indicate epicenter positions, depth (by color) and magnitude of EQs (by dimension), azimuthal distributions of radiation and positions of radiation sources, which are marked by thick green lines. Dashed lines depict boundaries of main lobes of radiation. Blue arrows show possible ways of gas emanation. It is visible that EQ epicenters are located in the direction of continent and approximately perpendicular to the radiation sources and accordingly axes of trenches. It is not always so for distant EQs (e.g., Fig. 12b, d).

We do not consider all possible positions of EQ epicenters for calculating distances based on the position of radiation source, because most of EQ epicenters lie in ~ 300 km width strip between Kuril–Kamchatka trench and peninsula coast. It does not create noticeable errors even when we assume that the boundaries of epicenter distances are approximately equal to the distances to the boundaries of radiation source. Zone of nearest Aleutian EQs is well known too and does not cause any problems in calculations.

Unfortunately, it is impossible to determine the exact position of the epicenter and depth of the focus and it is one of imperfections of our method. Although it seems that the shapes of precursors are visibly different for deep and shallow EQs, these dependences need a further careful study. Another method of determination of EQ focus position has been described as well as its application to the examples of two strong EQs (Kopytenko et al. 2006). It could be useful in addition to our method.

The algorithm for estimation of the local magnitude of a forthcoming EQ is considered in Sect. 2.4, which is based on the statistical dependence of local seismicity index K_{LS} for

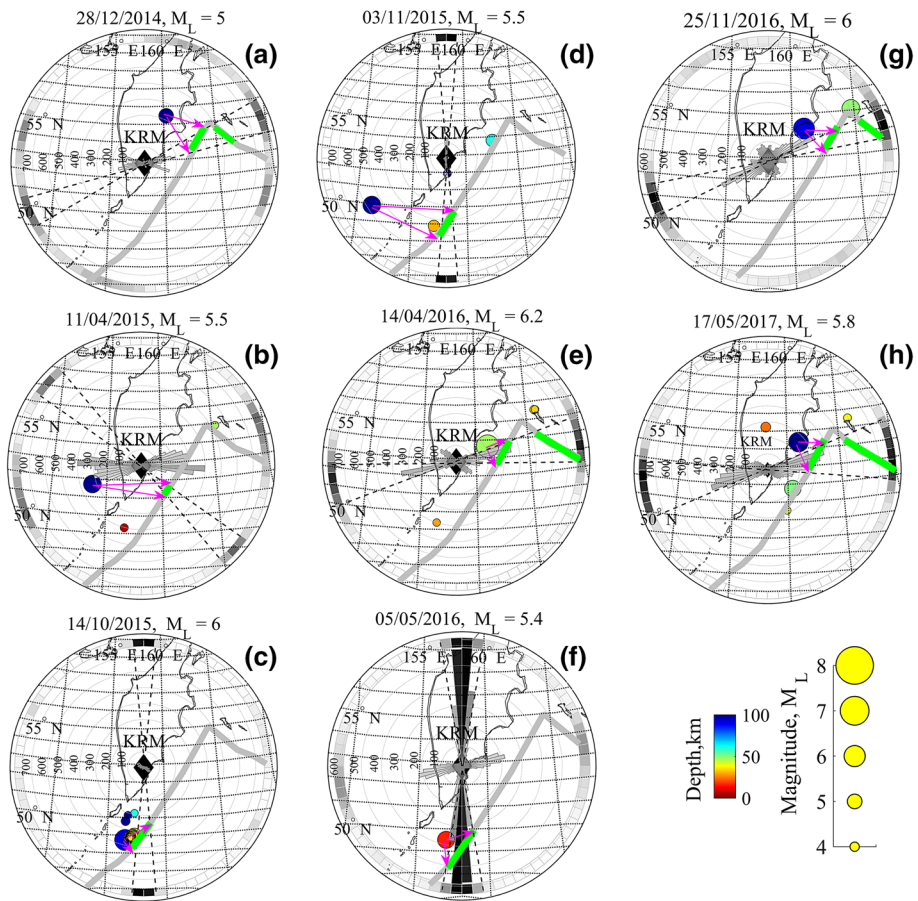


Fig. 12 Positions of EQ epicenters and sources of radiation depending on azimuthal distributions. Color circles indicate EQ epicenter positions. Their diameter and color depend on depth and magnitude. Two panels in right bottom angle display these relationships. Thick green lines mark sources of radiation. The dashed lines display azimuthal boundaries of maximum radiation

a forthcoming EQ on the preceding maximum value of ULF depression observed in either of two field components at frequencies 0.01–0.05 Hz. We found this phenomenon about 10 years ago (Schekotov et al. 2006) and have been working on this during these days (Schekotov and Hayakawa 2017). Here, we assume that the distance from the observatory to the EQ epicenter is approximately equal to that to the source of radiation (see Fig. 4). They roughly coincide with EQs, which are close to the trench and at latitudes, but noticeably differ in latitudes close to the latitude of the point of observation for events distant from the source of radiation. In other cases, there can appear considerable errors. Another possible source of errors is geomagnetic field. “Tail” of geomagnetic disturbances can decrease the value of ULF depression and value of the predicted magnitude, but it may happen only during very strong geomagnetic storms. In any case, it would be useful to add our observations with the use of geomagnetic field data.

We have considered ΔS as an indicator of EQ preparation process in Sect. 2.5, even though we do not know the origin of this phenomenon. One hypothesis consists in the

occurrence of ionospheric irregularity, which modifies the structure of background field. This irregularity can change the orientation of polarization ellipse and decrease its dispersion (Schekotov et al. 2007). Two components of ΔS make it possible to approximately estimate the position of this irregularity. It is reasonable to assume that its position is located under the region where gas is an outcome from the ocean. A source of ionospheric radiation should be located somewhere here too; however, a growth in ΔS can be observed without atmospheric radiation. Then, the value of ΔS does not connect with parameters of a forthcoming EQ. Errors of ΔS can occur due to natural emissions and industrial interferences at frequencies from units to tens Hertz. They can result in a growth in ΔS and as consequence become a cause of false alarms.

A possibility of rough estimation of occurrence time for a forthcoming EQ has been shown in Sect. 2.6. It does not coincide with our first astonishing and strange results obtained during the years of 2000–2004. At that time, we have shown based on rather good statistics that the mean delay of EQ date relative to preceding maxima of depression and ΔS was equal to about 3 days (Schekotov et al. 2006, 2007). Now, we see tailing of their distributions from a few days to a few months (see Fig. 8), which is probably connected with the evolution of local tectonics.

Results of an experiment on the EQ prediction described in Sect. 3 give some insight on possibilities of our method. We can conclude that most successfully we predict local magnitude and latitude of the epicenter and very approximately the time of future events.

Some errors in estimating EQ parameters can be caused by impossibility unambiguously to separate precursors of different events. In some cases, it would be easier to make full use of a few points of observation, and it is one of the most important steps in the future of this method.

We see that only this single method cannot give full-fledged prediction. It would be reasonable to expand this experiment using the collaboration with other promising tools, including method of EQ prediction based on seismic electric signals (Varotsos et al. 1993), VLF method (Hayakawa et al. 2010, Hayakawa 2011; Rozhnoi et al. 2013), remote sensing data from satellites (Pulinets et al. 2016), high frequency seismic noise (Saltykov et al. 2008) etc.

Acknowledgements We thank the whole staff of the Institute of Geophysical Survey RAS in Petropavlovsk-Kamchatsky for providing the data of magnetic fields and data of seismicity.

References

- Fowler RA, Kotick BJ, Elliot RD (1967) Polarization analysis of natural and artificially induced geomagnetic micropulsations. *J Geophys Res* 72:2871–2875
- Fraser-Smith AC, Bernardi A, McGill PR, Ladd ME, Helliwell RA, Villard OG (1990) Low-frequency magnetic field measurements near the epicenter of the $M_s = 7.1$ Loma Prieta earthquake. *Geophys Res Lett* 17:1465–1468
- Geller RJ, Jackson DD, Kagan YY, Mulargia F (1997) Earthquakes cannot be predicted. *Science* 275(5306):1616. <https://doi.org/10.1126/science.275.5306.1616>
- Gufeld IL, Matveeva MI, Novoselov ON (2011) Why we cannot predict strong earthquakes in the Earth's crust. *Geodyn Tectonophys* 2(4):378–415. <https://doi.org/10.5800/GT2011240051>
- Hattori K (2013) ULF geomagnetic changes associated with major earthquakes. In: Hayakawa M (ed) Earthquake prediction studies: seismo electromagnetics. TERRAPUB, Tokyo, pp 129–152
- Hayakawa M (2011) Probing the lower ionospheric perturbations associated with earthquakes by means of subionospheric VLF/LF propagation. *Earthq Sci* 24(6):609–637
- Hayakawa M (2015) Earthquake prediction with radio techniques. Wiley, Singapore, p 294p

- Hayakawa M, Kawate R, Molchanov OA, Yumoto K (1996) Results of ultra-low-frequency magnetic field measurements during the Guam earthquake of 8 August 1993. *Geophys Res Lett* 23:241–244
- Hayakawa M, Kasahara Y, Nakamura T, Muto F, Horie T, Maekawa S, Hobara Y, Rozhnoi AA, Solovieva M, Molchanov OA (2010) A statistical study on the correlation between lower ionospheric perturbations as seen by subionospheric VLF/LF propagation and earthquakes. *J Geophys Res* 115:A09305. <https://doi.org/10.1029/2009JA015143>
- Kopytenko YA, Matiashvily TG, Voronov PM, Kopytenko EA, Molchanov OA (1990) Discovery of ULF emission connected with the Spitak earthquake and its aftershock activity on data of geomagnetic pulsations observed at Dusheti and Vardiziya, *IZMIRAN Preprint* N3(888), p 27, Moscow (in Russian)
- Kopytenko YA, Ismaguilov VS, Hattori K, Hayakawa M (2006) Determination of hearth position of a forthcoming strong EQ using gradients and phase velocities of ULF geomagnetic disturbances. *Phys Chem Earth* 31:292–298
- Molchanov OA, Hayakawa M (2008) Seismo-electromagnetics and related phenomena. History and latest results. TERRAPUB, Tokyo
- Molchanov OA, Kopytenko YA, Kopytenko EA, Matiashvilli T, Fraser-Smith AC, Bernardi A (1992) Results of ULF magnetic field measurements near the epicenters of the Spitak ($M_s=6.9$) and Loma Prieta ($M_s=7.1$) earthquakes: comparative analysis. *Geophys Res Lett* 19:1495–1498
- Pulinets SA, Ouzounov DP, Karelin AV, Davidenko DV (2015) Physical bases of the generation of short-term earthquake precursors: a complex model of ionization-induced geophysical processes in the lithosphere–atmosphere–ionosphere–magnetosphere system. *Geomagn Aeron* 55(4):540–558. <https://doi.org/10.1134/S0016793215040131>
- Pulinets S, Ouzounov D, Davydenko D, Petrukhin A (2016) Multiparameter monitoring of short-term earthquake precursors and its physical basis. In: Implementation in the Kamchatka region. E3S Web of Conferences 11, 00019. <https://doi.org/10.1051/e3sconf/20161100019>
- Rozhnoi A, Solovieva M, Hayakawa M (2013) VLF/LF signals method for searching of electromagnetic earthquake precursors. In: Hayakawa M (ed) Earthquake prediction studies: seismo electromagnetics. TERRAPUB, Tokyo, pp 31–48
- Saltykov VA, Kugaenko YA, Sinityn VI et al (2008) Precursors of large Kamchatka earthquakes based on monitoring of seismic noise. *J Volcanol Seismol* 2:94. <https://doi.org/10.1134/S0742046308020036>
- Schekotov A, Hayakawa M (2017) ULF/ELF electromagnetic phenomena for short-term earthquake prediction. LAP LAMBERT Academic Publishing, p 102, ISBN 978-3-330-06286-3
- Schekotov A, Molchanov O et al (2006) Seismo-ionospheric depression of the ULF geomagnetic fluctuations at Kamchatka and Japan. *Phys Chem Earth* 31:313–318
- Schekotov AY, Molchanov OA, Hayakawa M et al (2007) ULF/ELF magnetic field variations from atmosphere induced by seismicity. *Radio Sci* 42:RS6S90. <https://doi.org/10.1029/2005rs003441>
- Schekotov AY, Molchanov OA, Hayakawa M et al (2008) About possibility to locate an EQ epicenter using parameters of ELF/ULF preseismic emission. *Nat Hazards Earth Syst Sci* 8:1237–1242
- Schekotov A, Fedorov E, Molchanov O, Hayakawa M (2013) Low frequency electromagnetic precursors as a prospect for earthquake prediction. In: Hayakawa M (ed) Earthquake prediction studies: seismo-electromagnetics. TERRAPUB, Tokyo, pp 81–99
- Uyeda S et al (2002) Japanese–Russian complex geophysical observatory in Kamchatka region for monitoring of phenomena connected with seismic activity. In: Hayakawa M, Molchanov O (eds) Seismo-electromagnetics (Lithosphere–Atmosphere–Ionosphere coupling). TERRUPUB, Tokyo, pp 433–443
- Varotsos P, Alexopoulos K (1984) Physical properties of the variations of the electric field of the earth preceding earthquakes. *I. Tectonophysics* 110(1–2):73–98
- Varotsos P, Lazaridou M (1991) Latest aspects of earthquake prediction in Greece based on seismic electric signals. *I. Tectonophysics* 188:321–347
- Varotsos P, Alexopoulos K, Nomicos K, Lazaridou M (1986) Earthquake prediction and electric signals. *Nature* 322:120
- Varotsos P, Alexopoulos P, Lazaridou M, Nagao M (1993) Earthquake predictions issued in Greece by seismic electric signals since February 6, 1990. *Tectonophysics* 224:269–288
- Varotsos PV, Sarlis NV, Skordas ES (2003) Electric fields that “arrive” before the time-derivative of the magnetic field prior to major earthquakes. *Phys Rev Lett* 91:148501

Affiliations

A. Schekotov¹  · D. Chebrov² · M. Hayakawa^{3,4} · G. Belyaev⁵ · N. Berseneva⁶

D. Chebrov
danila@emsd.ru

M. Hayakawa
hayakawa@hi-seismo-em.jp

G. Belyaev
belyaev@izmiran.ru

N. Berseneva
nataberskam@gmail.com

- ¹ The Schmidt Institute of Physics of the Earth of the Russian Academy of Sciences (IPE RAS), 10-1 B. Gruzinskaya, Moscow, Russia 123242
- ² Kamchatka Branch of Geophysical Survey of Russian Academy of Sciences, KB GS RAS, Petropavlovsk-Kamchatski, Russia
- ³ Hayakawa Institute of Seismo Electromagnetics, Co. Ltd. (Hi-SEM), UEC (University of Electro-Communications), Alliance Center #521, 1-1-1 Kojima-cho, Chofu, Tokyo 182-0026, Japan
- ⁴ Advanced Wireless & Communications Research Center (AWCC), UEC, 1-5-1 Chofugaoka, Chofu, Tokyo 182-8585, Japan
- ⁵ Pushkov Institute of Terrestrial Magnetism, Ionosphere and Radiowave Propagation (IZMIRAN), RAS, Troitsk, Kaluzhskoe Hwy 4, Moscow, Russia 108840
- ⁶ Lomonosov Moscow State University, 1-2 Leninskie Gory, Moscow, Russia 119991